Herbert R. Weischedel
NDT Technologies, Inc., South Windsor, CT, USA

Wire Rope Roughness (WRR), a new indicator for the quantitative characterization of wire rope deterioration

Summary

While widely used for making retirement decisions, loss of metallic cross-sectional area (LMA) by itself is frequently not a good indicator of the actual wire rope condition. For example, wire fatigue breaks, single or in clusters, cause little or no LMA. Similarly, while corrosion pitting is associated with little loss of material, it is insidious because it damages the deep structure of the metal.

To remedy this situation, this paper introduces the concept of **Wire Rope Roughness (WRR)** as an additional quantitative indicator. WRR is defined as the aggregate roughness of all wires in a rope including broken wires and corrosion pitting.

WRR is derived and extracted from the LMA signal in the following steps:

- Rope inspection and acquisition of a *high-resolution* LMA signal.
- Using the distance counter signal to produce a distance-based LMA signal.
- Removing measurement artifacts from the LMA signal by using the so-called *echo cancellation (signal enhancement)* algorithm to produce a *high-fidelity* LMA signal.
- Extracting a (high-fidelity) WRR signal from the high-fidelity LMA signal by a nonlinear, high-pass filter-like algorithm.

Illustrated by examples, the paper describes the above steps in detail.

1 Introduction

The operating safety of wire ropes is adversely affected by several types of rope deterioration. For the purposes of this paper, major deterioration modes can be categorized as follows.

Basic Loss of Metallic Cross-Sectional Area (BLMA):
BLMA is loosely defined as Loss of Metallic Cross-Sectional Area that changes gradually and smoothly over extended distances (say, greater than one Lay Length) along the length of a rope. The BLMA signal is characterized by slow – i.e., low spatial frequency – variations over long distances along the rope. While for the purposes of this paper, BLMA is mostly a theoretical concept, for actual ropes this type of damage is usually caused by wear and corrosion assisted wear.

Wire Rope Roughness (WRR):
WRR is defined as the aggregate surface roughness of all wires in a rope. WRR is typically caused by and indicates corrosion pitting, interstrand nicking, broken wires and clusters of broken wires. The WRR signal is characterized by small-amplitude and rapid – i.e., high spatial frequency – variations over short distances along the rope.

2 Wire rope deterioration modes of the WRR-type [1], [2], [3], [4]

The following examples describe some typical rope deterioration modes of the WRR-type that are the subject of this paper.

2.1 Corrosion pitting

Corrosion is a serious hazard to a wire rope.

Corrosion pitting causes stress concentrations. This kind of corrosion is extremely insidious, as it causes little loss of material with rather small effects on the rope surface, while it damages the deep structures of the metal. The pits on the wire surfaces are often covered by corrosion products.

Corrosion pitting inhibits the free movement of wires and strands, which produces additional stresses in wires. The increased wire stresses combined with the above mentioned stress concentrations can drastically accelerate the development of fatigue breaks.

Corrosion assisted wear can also cause wires to corrode uniformly over their entire surface which may reduce their cross-sectional area and cause loose wires.

The severity of corrosion often varies along the length of a rope. Frequently, corrosion is localized but, nevertheless, dangerous. The extent of corrosion is often difficult to gauge and – as shown by experience – is usually underestimated.

2.2 Internal broken wires (single and in clusters), interstrand nicking

Many ropes are of the torque-balanced multistrand type, comprising two or more layers of strands. Figure 1 shows a cutaway section of such a rope. Torque balance is achieved in multistrand ropes by laying outer and inner strands in opposite directions.

This type of rope construction limits axial rotation of a freely suspended rope under load. In addition, multistrand ropes offer flexibility and a wear resistant surface profile.

In single fall crane operations the use of non-rotating ropes is mandatory.

However, the wires and strands in different layers of these ropes touch locally and at an angle. Therefore, when multistrand ropes bend over sheaves or on a drum, they are subject to the combined effect of radial loading, relative motion between wires and bending stresses.

Therefore, multistrand ropes are prone to develop interstrand nicking (Figures 2 and 3) and, eventually, internal broken wires (Figure 4). This breakup occurs primarily on the interface between the outer and second layer of strands, usually with no externally visible signs as indicated by Figure 5. The wires in the second layer of strands typically show nicking and breaks caused by a combination of fluctuating axial wire stresses, interwire motions and fluctuating radial loads. The broken wires usually show squared-off and z-shaped ends that are typical for fatigue breaks.

Figure 1: Multistrand rope

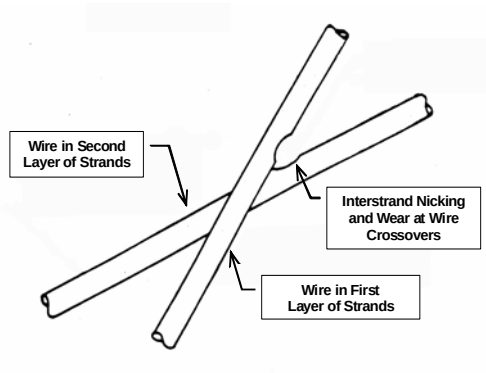

Figure 2: Interstrand nicking

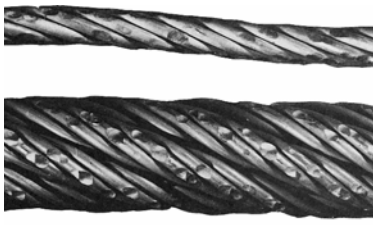

Figure 3: Interstrand nicking

Figure 4: Broken wires in second layer of trands

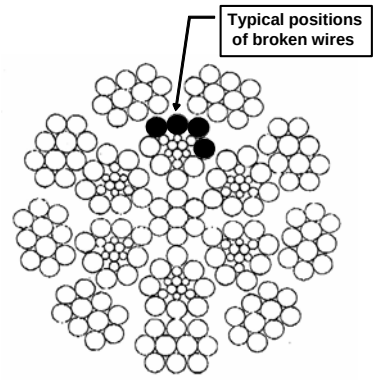

Figure 5: Typical positions of broken wires in multistrand ropes

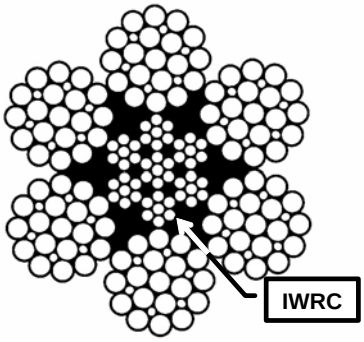

Figure 6: IWRC rope construction

Similar nicking and fatigue patterns occur also in IWRC (Independent Wire Rope Core) ropes. Figure 6 shows a typical cross-sectional diagram of such a rope. For IWRC ropes, the outer wires of the outer strands have a larger diameter than the outer core strand wires. To minimize interstrand nicking between the outer strands and the IWRC, these ropes are designed such that the wires of the outer strands and the IWRC are approximately parallel. (This is usually achieved by choosing a *Lang lay* construction for the IWRC and an *ordinary lay* construction for the outer strands.)

Typically, the wires of the outer strands are well supported by their neighbors while the outer wires of the IWRC are relatively unsupported.

The result of these geometrical features is that, under fluctuating tensile loads, the outer IWRC wires are continuously forced into the valleys between the outer strand wires and then released. This mechanism results in secondary bending stresses leading to large numbers of core wires with fatigue breaks. These breaks can be very close together and can form groups of breaks. Eventually, the IWRC can break, or it can even completely disintegrate into short pieces of wire about half a lay length long. This condition is commonly called *complete rope core failure.*

As the IWRC fails, the outer strands lose their radial support. This allows the wires of the outer strands to bear against each other tangentially. The resulting interstrand nicking restricts the movement of the strands within the rope. Without this freedom of movement, secondary fatigue breaks in the wires of the outer strands will develop at the strand tangent points. Because these fatigue breaks develop in the valleys between the outer strands, they are also called *valley breaks* (Figure 7).

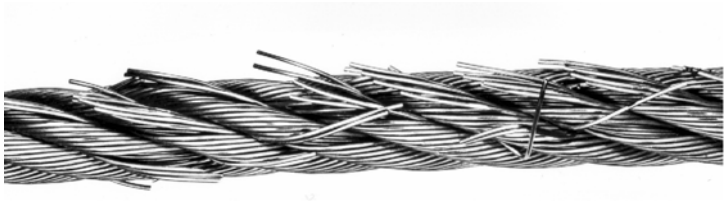

Figure 7: Valley breaks

2.3 Spiral strand

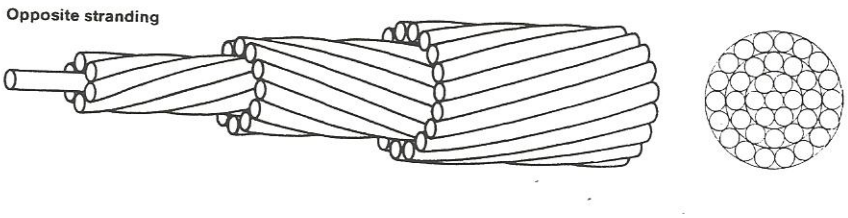

Figure 8: Spiral strand construction

Spiral strand (Figure 8) is made up of concentric layers of wires, some of which are spun in opposing directions to give the strand a measure of torque balance. Therefore, the individual wires in different layers touch locally and at an angle, and the helical geometry within the layers creates radial interlayer contact forces. When used in mooring applications, spiral strand is subject to fluctuating loads and, especially, bending. Then, depending on the level of axial tension and radius of curvature, spiral strand is subject to interlayer slippage, which causes axial motion between wires in different layers combined with tension and torque stresses. Therefore, it is to be expected that, as a result of these geometrical features, wires in different layers will develop interwire nicking and fretting and, eventually, secondary fatigue breaks.

As an aside, spiral strand is frequently protected by plastic sheathing, which prevents corrosion and corrosion pitting. However, plastic sheathing makes visual inspections ineffective.

2.4 Quantitative characterization of broken wires and broken wire clusters

The detailed detection and quantitative characterization of internal broken wires in ropes with many broken wires and clusters of broken wires pose problems.

Difficulties are caused by the fact that, for magnetic flux wire rope NDE, the indication of broken wires is influenced by a number of parameters like

- broken wire cross-sectional area,
- broken wire gap width, and
- the position of broken wires within the cross-section of the rope.
- For clusters of broken wires, an additional problem is caused by the fact that the relative position of broken wires with respect to each other along the length of the rope is not known. For example, the gaps of broken wires could be aligned or staggered.
- Finally and most importantly, broken wires with zero or tight gap widths are not detectable by nondestructive magnetic flux inspections because they do not produce a sufficient magnetic leakage flux.

Considering the above, wire rope NDE allows only an estimate of the number of broken wires.

3 Underlying Principles and Instrumentation

For all wire rope NDE instruments, strong permanent magnets induce a magnetic flux, at the saturation level, in the rope in the axial (longitudinal) direction. Various types of sensors, such as coils or Hall sensors close to the rope sense and measure the magnetic flux.

When a rope is magnetically saturated, the axial magnetic flux in the rope is proportional to its cross-sectional area. Therefore, any LMA (loss of metallic cross-sectional area) can be determined by measuring this magnetic flux.

For many rope testers, the so-called LF (localized flaw, localized discontinuity) signal is the first derivative of the rope cross-section signal. For other instruments, the LF signal is the second derivative of the rope cross-section, shown as *Alternative LF Signal*.

This is illustrated by Figure 9, which depicts the rope cross-section as the input signal.

In this context, *step changes of metallic cross-sectional area* – caused by missing or added wires, for example – have particular significance. Because of its simple geometry, a *step change* can be called a *fundamental defect*. Accordingly, the corresponding LMA and LF signals, caused by a *fundamental defect*, can be called *fundamental LMA* or *LF signals*, respectively. The *fundamental signals* can also be called an instrument's *step response.*

The idealized corresponding LMA and LF output signals are also shown in Figure 9. For many rope testers, the LF signal is the first derivative of the rope cross-section signal. For other instruments, the LF signal is the second derivative of the rope cross-section, as shown as *Alternative LF Signal* in Figure 9.

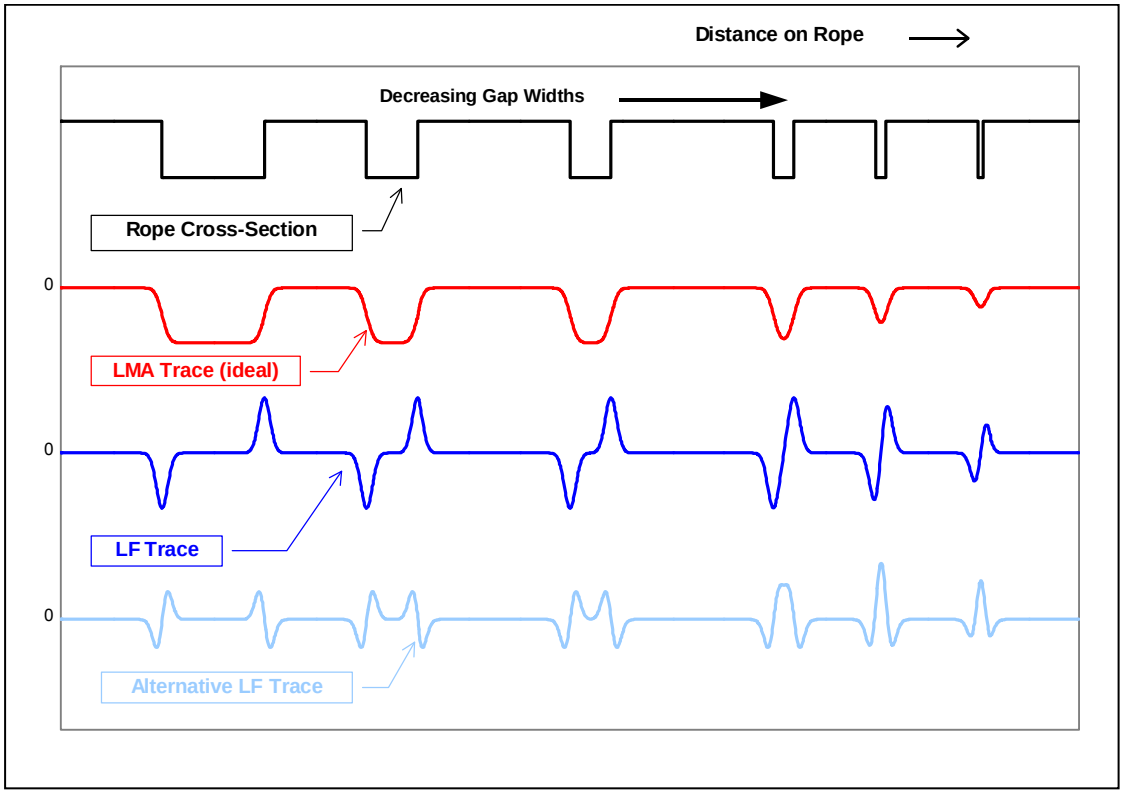

Figure 9: Input and output signals of an idealized rope test instrument

Any inspection equipment should present data in a form that facilitates their interpretation by the human operator.

A perfect LMA signal, such as shown in Figure 9, can serve as an accurate and conceptually simple map of a rope's LMA that is easy to interpret by the inspector. For the purposes of this paper, highly accurate LMA signals of the type in Figure 9 will be defined as *'high fidelity'* signals.

Unfortunately, actual LMA signals are far from this ideal. Most rope testers can produce LF signals with wave-shapes that are very similar to those of Figure 9. However, producing an LMA signal that comes close to the idealized LMA signal in Figure 9 poses problems.

The LF signal is frequently used for the detection of broken wires. However, Figure 9 shows that a typical LF chart recorder signal of a broken wire has positive and negative going sections. Therefore, positive and negative signal components, caused by closely spaced broken wires in a cluster, have a tendency to, and will, overlap and cancel. This idiosyncrasy makes it impossible to determine – or even estimate – the number of broken wires in a cluster. Therefore, the LF signal is of limited use for estimating the number of broken wires in clusters and will not be discussed in further detail.

3 Wire rope roughness (WRR) analysis

WRR is derived and extracted from the LMA signal in the following steps:

- Rope inspection and acquisition of a *high-resolution* LMA signal.
- Using the distance counter signal to produce a distance-based LMA signal.
- Removing measurement artifacts from the LMA signal by using the so-called *echo cancellation (signal enhancement)* algorithm to produce a *high-fidelity* LMA signal.
- Extracting a (high-fidelity) WRR signal from the high-fidelity LMA signal by a nonlinear, high-pass filter-like algorithm.

The stages of the WRR analysis process are illustrated by Figure 10 that shows a functional diagram of the WRR extraction process. The following discussion describes these steps.

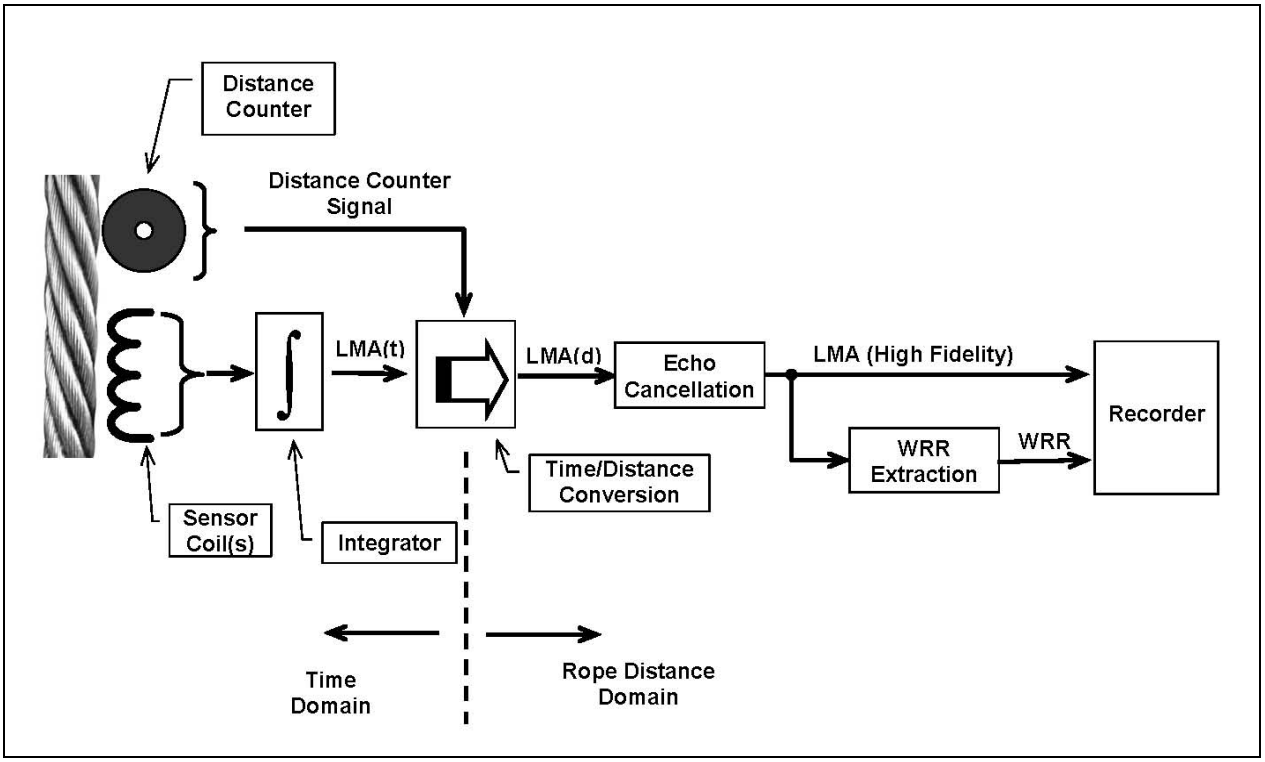

Figure 10: Wire rope roughness (WRR) analysis

3.1 Wire rope inspection and LMA signal acquisition

For all wire rope test instruments, strong permanent magnets induce a magnetic flux at the saturation level in the rope in the axial (longitudinal) direction.

When a rope is magnetically saturated, the axial magnetic flux in the rope is proportional to its cross-sectional area. Therefore, any LMA (loss of metallic cross-sectional area) can be determined by measuring this magnetic flux.

As indicated in Figure 10, coils close to the rope sense and measure the magnetic flux. Essentially, there are two different coil arrangements that can be used: *Annular coils* and *modified coils*, each with distinct advantages and disadvantages [**2**].

Since coils sense only the time derivative of the magnetic flux, the coil signals must be integrated to actually determine the magnetic flux in the rope. Therefore, a coil-cum-integrator approach is used to measure this magnetic flux and to obtain the experimental results of the present paper.

If combined with *echo cancellation* or *signal enhancement* [**5**]**,** the coil-cum-integrator approach offers *high-fidelity* LMA signals with exceptional resolution as required for a WRR analysis.

Note that integration of the coil signal is performed in the time domain.

3.2 Distance based LMA signal

The coil-cum-integrator flux detector produces a time-based LMA signal. On the other hand, to perform a WRR analysis, a distance-based signal is required.

Therefore, using the distance counter signal, the time/distance transformation of the LMA signal is performed by the time/distance converter in Figure 10. All further conditioning of the LMA signal is then performed in the *rope distance domain*.

3.3 Echo cancellation (signal enhancement)

As will be demonstrated by the following examples, WRR is a reliable indicator of the rope condition. Because it is derived from the LMA trace, WRR is automatically calibrated together with the LMA signal (say, in % of metallic rope cross-sectional area). Therefore, the WRR trace can be used to quantitatively characterize corrosion pitting and external and internal broken wires, including clusters of broken wires. Especially, in the absence of corrosion pitting, WRR Analysis is well suited for estimating the number of internal and external broken wires (single or in clusters).

3.3.1 LMA signal artifacts

The WRR Analysis method extracts the WRR signal from the LMA signal. Compared to the LMA signal, WRR signal amplitudes are usually quite small.

On the other hand, nondestructive wire rope test equipment frequently introduces – avoidable or sometimes unavoidable – instrument-specific artifacts into the test signals. While these artifacts represent relatively minor disturbances for the overall LMA signal, their signal amplitudes are of the same order of magnitude as those of the WRR signal. Hence, if not eliminated and/or avoided, they seriously distort the rather small WRR signal, and they will compromise the accuracy and reliability of WRR test results.

For example, low-pass filtering is typically used to reduce inherent noise and to make LMA signals visually acceptable. However, low-pass filters make inspection results dependent on inspection speed, and they suppress and distort the relatively small indications caused by corrosion pitting and broken wire clusters. These indications always have high spatial-frequency components, and the amplitudes of test signals with high frequencies are drastically reduced by low-pass filtering. Hence, low-pass filtering must be avoided for WRR Analysis.

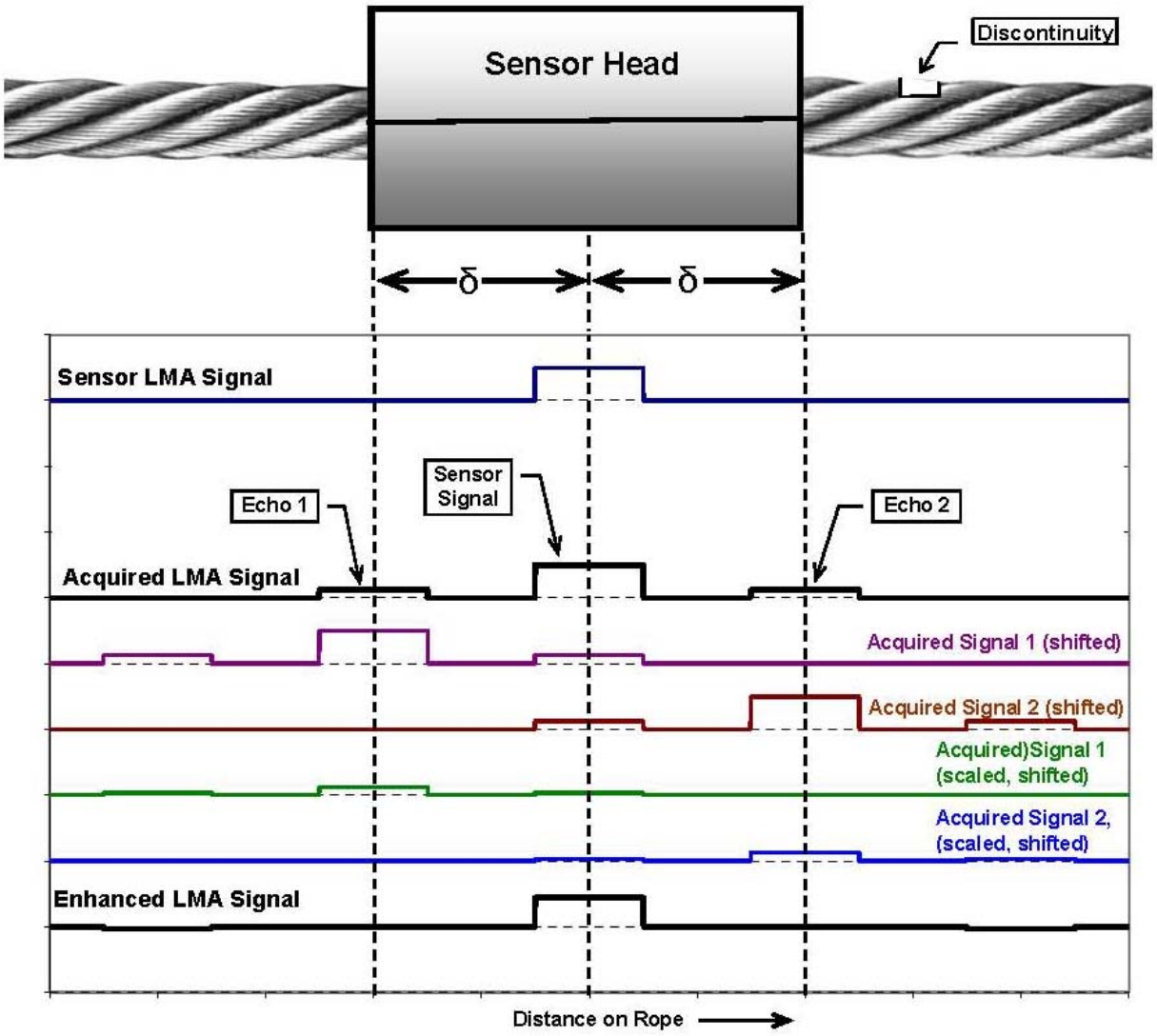

Figure 11: Echo Effect and echo cancellation

Other artifacts are introduced by the physics of the data acquisition process.

One of these phenomena is called the 'Echo Effect', which can be explained as follows (see Figure 11).

A particular discontinuity causes its actual indication in the test signal as it passes the sensor-section that is positioned in the center of the test head. Two echoes – with smaller amplitudes than the actual indication – are induced when this discontinuity enters and exits the sensor head. Hence, the 'echoes' occur immediately before and after the actual signal indication.

Assuming the sensor head has an overall length of 2δ as shown in Figure 11, the primary sensor signal occurs when the discontinuity passes the detector coils at the center of the head. Secondary echo signals (Echo 1 and Echo 2) occur, respectively, when the defect enters and leaves the sensor head.

The *Echo Effect* is inherently caused by the geometry of the sensor-magnet arrangement – with the sensor section positioned between the two poles of a permanent magnet. This basic design is common to all present-day sensor heads of the hinged clamshell design. Therefore, any of the present sensor heads will exhibit this behavior.

While the echoes introduce measurement errors that are relatively small compared to the LMA signal, they represent a significant distortion for the WRR signal, and they should be eliminated if at all possible.

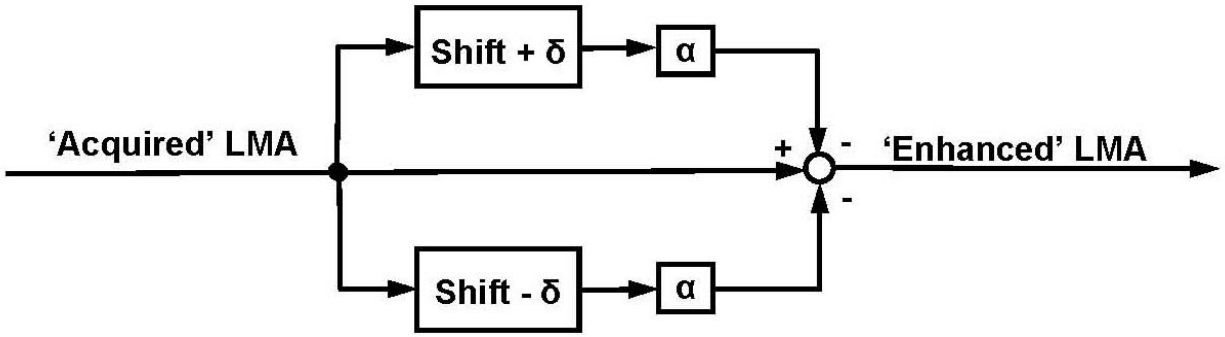

Figure 12: Echo cancellation algorithm

The 'echoes' can be drastically reduced by an *echo cancellation* – or *signal enhancement* – computer algorithm. This procedure is explained as follows.

As illustrated by Figures 11 and 12, the acquired LMA signal is first shifted by rope distances +δ and –δ, respectively. Then the two shifted signals are multiplied by a factor α<1 (frequently α = 0.25) and then subtracted from the acquired LMA signal to produce the *enhanced LMA signal*.

Signal Enhancement allows test signals with exceptional fidelity and resolution.

This added degree of accuracy becomes meaningful if and when WRR Analysis will be used to make rope retirement decisions. Then, the extra precision will become significant for avoiding either premature rope retirement or unsafe operating conditions.

The *echo cancellation* algorithm has been implemented as part of a signal analysis computer program, and it is now routinely used for analyzing the results of magnetic flux wire rope inspections.

To illustrate the echo cancellation method, Figures 13.1 - 13.3 show the LMA and LF traces of a laboratory test rope. The LMA and LF signals were acquired with *annular coils* and *modified coils* as described in [**2**].

For these experiments, short pieces of wire, attached to the rope, simulate anomalies. The attached wires have different lengths as indicated. They typically represent a 1% increase of metallic cross-sectional area. (The LMA caused by the internal wire is unknown). The two ends of the rope are welded together to form an infinite loop. The LMA caused by the weld is also indicated in the chart.

Figure 13.1 shows the excellent results that could be obtained with annular coils. This means, the increases of metallic cross-sectional area, caused by the attached wires, are clearly indicated with their full magnitude of 1% for wires that are longer than about 50 mm. The metallic cross-sectional area changes caused by shorter wires are also indicated, albeit – due to the limited resolution of the signal acquisition process – not to their full extent.

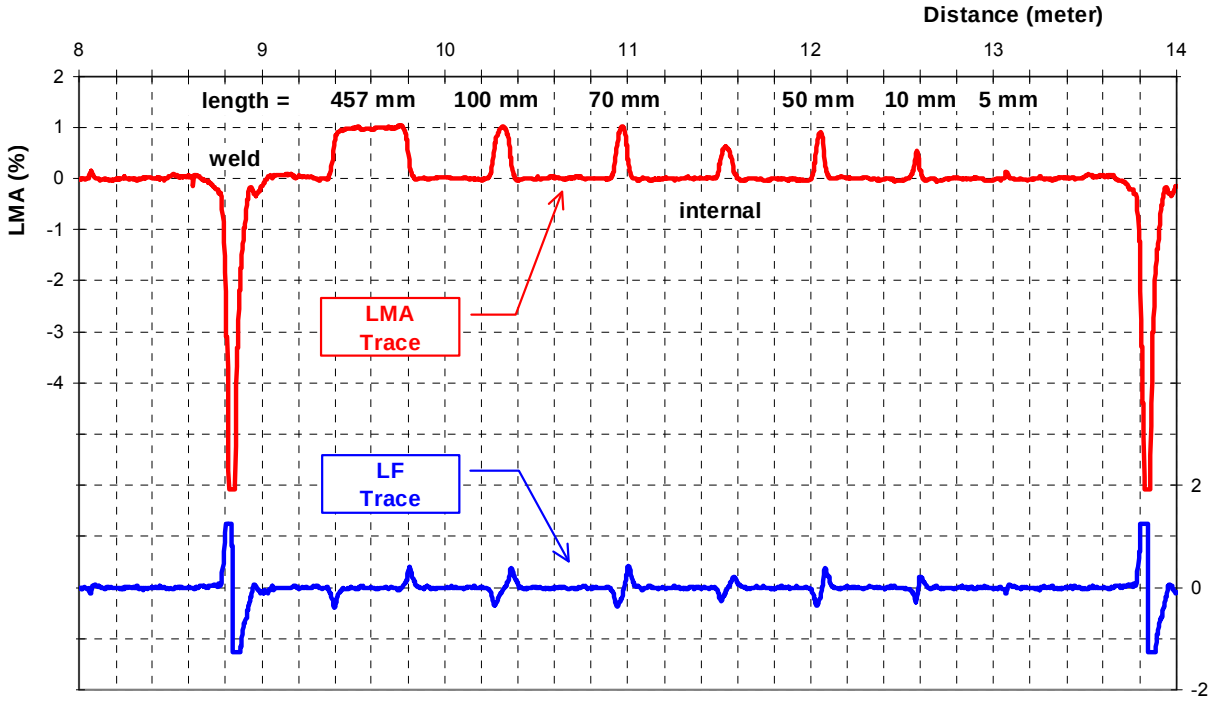

Figure 13.1: Step responses for annular coil method

These test results show that the *annular coil* approach offers uncommon resolution and *signal fidelity*. In fact, the test signals of this method closely resemble the idealized results of Figure 9. Note, however, that the *annular coil* method is not practical for actual inspections in the field [**2**].

Figure 13.2 shows the test signal generated by the *modified coil* method. This approach is practical and useful for field inspections. As mentioned in reference [**2**], the test signals of this *modified coil* method are a combination of the *annular coil* signal and a signal component that is caused by the (parasitic) outside stray flux, i.e., that portion of the flux that leaves and enters the sensor head to and from the outside and flows along some external stray flux path. Unfortunately, this outside signal component is significant. It compromises the quality of the test results and must be considered parasitic.

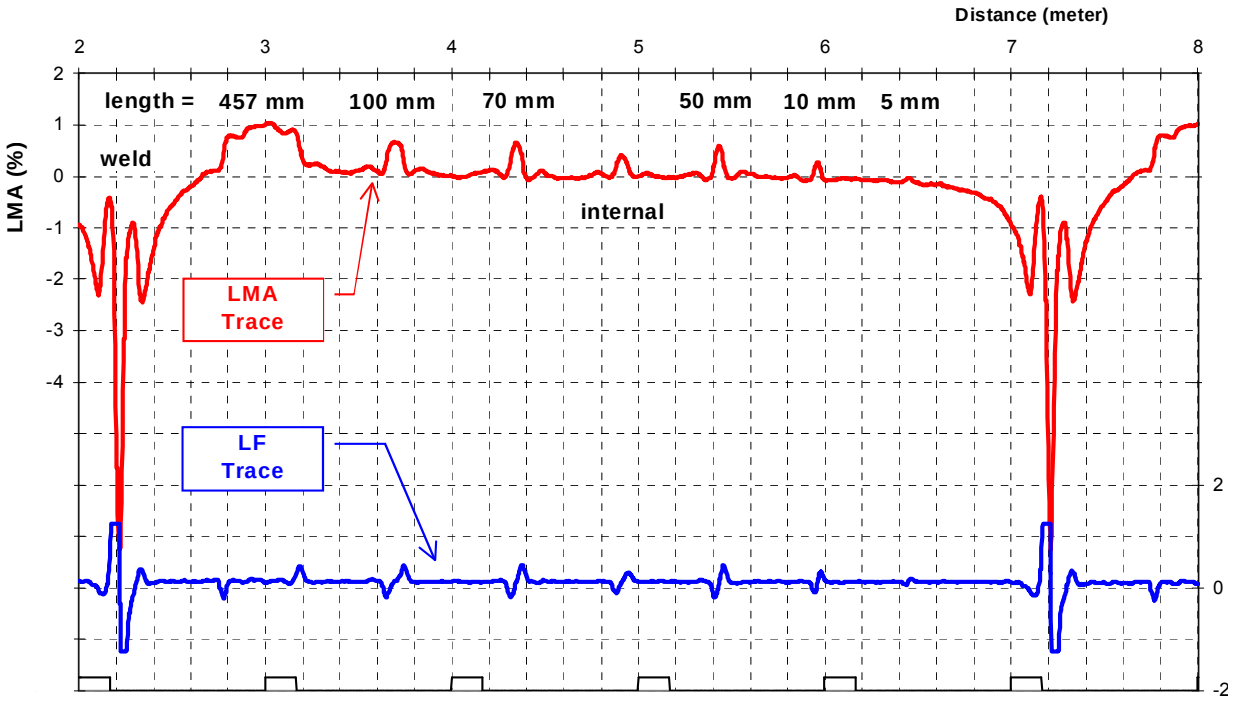

Figure 13.2: Step responses for modified coil method

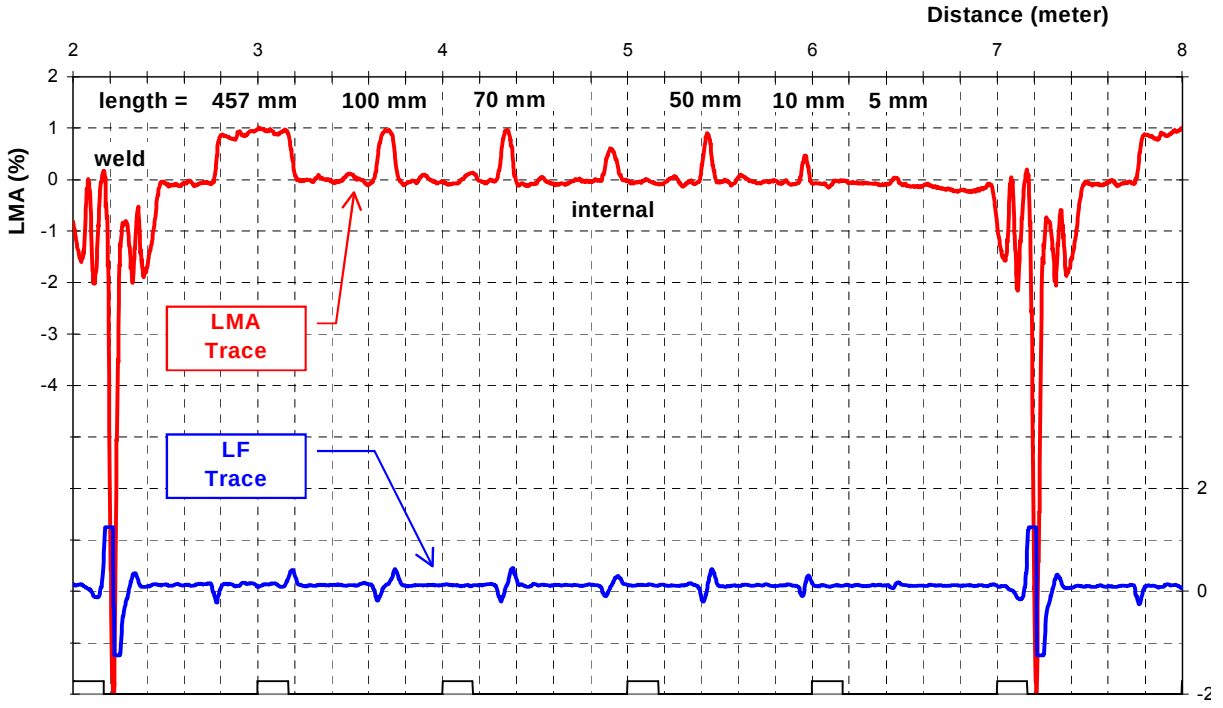

Figure 13.3: Step responses for Modified Coil method after Echo Cancellation

As mentioned previously, this outside signal component is generated as a rope discontinuity enters and leaves the sensor head, respectively. The parasitic outside signal components resemble the main signal component with smaller amplitude as illustrated by Figure 13.2.

Fortunately, the physics of this parasitic effect is well understood. It can be minimized by using the above-described *echo cancellation* or *signal enhancement* procedure.

Signal enhancement is illustrated by Figures 13.2 and 13.3. Figure 13.2 shows the LMA trace before *signal enhancement* that was acquired with a sensor head of the *auxiliary coil* type. Here, the indicated change of cross-section depends on the length of the anomaly as illustrated. This means that area changes caused by short anomalies are not indicated to their full extent. Figure 13.3 shows that, after enhancement (with the above-mentioned *enhancement algorithm*), all metallic area changes that extend over lengths greater than 50 mm are correctly measured. In other words, the *averaging length* (or *quantitative resolution*) [**2**] is now 50 mm, which equals the quantitative resolution of the annular coil approach illustrated by Figure 13.1. This means that the LMA trace of Figure 13.3 qualifies as a *high-fidelity* signal.

The *Signal Enhancement* algorithm is further illustrated as part of Test 2 below.

3.2 WRR and BLMA extraction

The LMA signal consists of two components, the BLMA signal and the WRR signal. The WRR analysis method extracts these components from the LMA signal in order to analyze, determine and measure WRR and BLMA.

The WRR signal is characterized by relatively small-amplitude and rapid – i.e., high spatial frequency – random variations over short distances (typically less than a lay length) along the rope.

Conversely, the BLMA signal is characterized by random variations with variable amplitudes and rather slow – i.e., low spatial frequency – random fluctuations over relatively long distances (typically longer than a lay length) along a rope.

As defined above, the WRR signal is superimposed on the BLMA signal to comprise the LMA signal.

The spatial-frequency ranges of the BLMA and WRR signal components, respectively, are very distinct and separated by a considerable gap.

The WRR extraction process is illustrated by Figure 14 that shows an idealized schematic representation of the LMA, WRR and BLMA signals (denoted “LMA”, “WRR” and “BLMA”, respectively). In the Figure, the WRR signal is represented by a single high-frequency low-amplitude sinusoidal signal – denoted “WRR” – while the BLMA signal is shown as a single low-frequency sinusoidal component called “BLMA”.

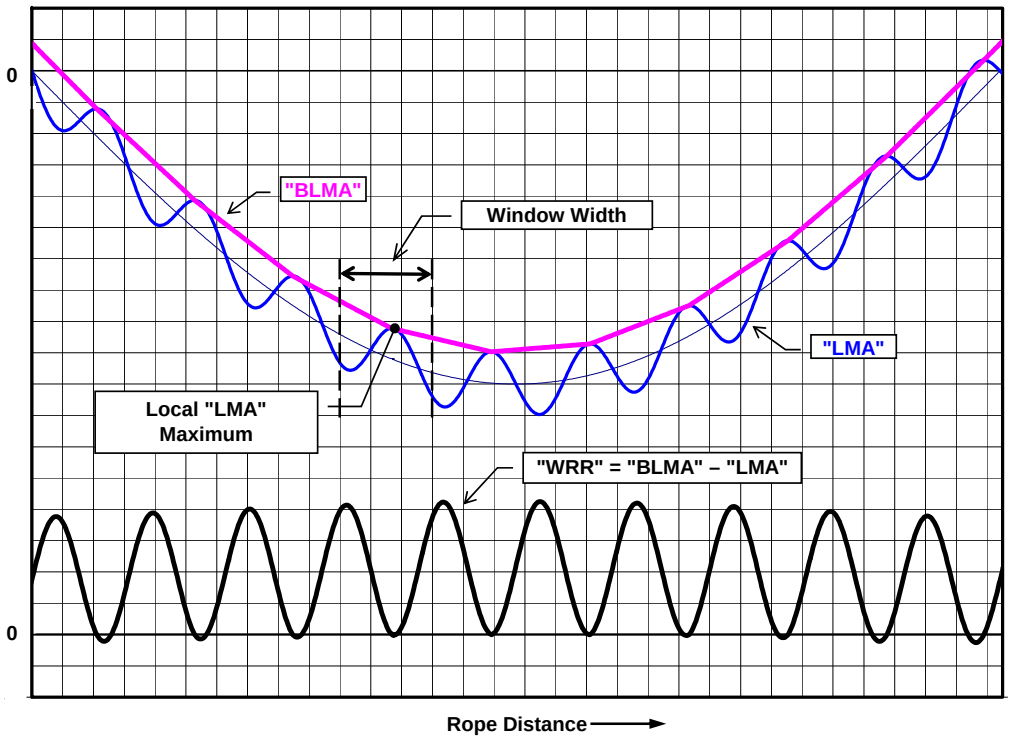

Figure 14: WRR analysis, schematic

Local (or relative) maxima of “LMA” over a certain sliding interval (or ‘window’) along a rope are then found as illustrated by Figure 14. The local maxima are established by scanning the rope along its entire length using a sliding window on the rope, and by determining the maximum values of the LMA signal within the sliding window. The width of the window can be specified by the inspector. Typically, the lay length of the rope under test can be used as window width. Note that the WRR Analysis shows little or no sensitivity to window width as long as this length is chosen to be approximately equal – within a certain range – to the rope lay length.

“BLMA” is then determined by finding the envelope of the “LMA” signal. For example, this can be done by interpolating between the local maximum points of the “LMA” signal.

“WRR” is calculated by subtracting “LMA” from “BLMA” as indicated in Figure 14.

A wide variety of procedures can be used for finding the relative maxima and for interpolation. All reasonable methods will produce similar results. For example, even a simple manual “eyeballing” method would be feasible for finding the relative maximum points and the envelope of an LMA signal.

4 Experimental results

NDT Technologies, Inc. has participated in several Round Robin tests. In the following, results from these experimental inspections will be used to establish feasibility of the WRR method.

These trials and the subsequent analysis of the test data were carried out in three stages.

- Test data were acquired by using nondestructive wire rope inspection equipment.
- The ropes under test were destranded after their examination, and the state of their deterioration was verified visually and recorded in great detail. These reports are in the public domain, and they are readily available [**6**], [**7**]**.**
- More recently, a WRR analysis of the test data was performed.

The correlation of the WRR Analysis results with the actual condition of the ropes under test shows a very close correspondence. This proves the feasibility and the value of the proposed methods.

4.1 Test 1

Test 1 concerns the WRR Analysis of the "Broken Wire Rope Sample" that was tested as part of Round Robin tests in Bochum (Germany) in 1998 [**6**].

This rope – referred to as Rope 1 in the following – had been used as a mine hoist rope on a trial basis and was known to contain numerous internal broken wires and no corrosion along its entire length.

Rope 1 is a 48 mm diameter, 15 strand, fishback, low rotation multi-layer rope. A cross-sectional diagram of the rope is shown in Figure 5. The present analysis deals with the inspection of this torque balanced multistrand rope.

This case study illustrates the use of WRR Analysis for the detection and quantitative characterization of internal broken wires and clusters of broken wires in multistrand ropes. The task at hand was to determine the number and position of broken wires along the length of the rope.

After the tests, a particular section of this rope was dismantled and carefully examined. This particular visual rope inspection is unique because it meticulously analyses and documents the actual rope condition in great detail. To our knowledge, no other rope has been as thoroughly examined as this one. A complete documentation is presented in the literature [**6**].

Figure 15 shows a WRR Analysis of the rope under test. This chart shows three traces as follows.

LMA(%) – The original LMA trace after Signal Enhancement.

BLMA(%) – The idealized Basic LMA trace without the effects of corrosion pitting and broken wires.

WRR(%) (Wire Rope Roughness) – A quantitative indication of corrosion pitting and broken wires.

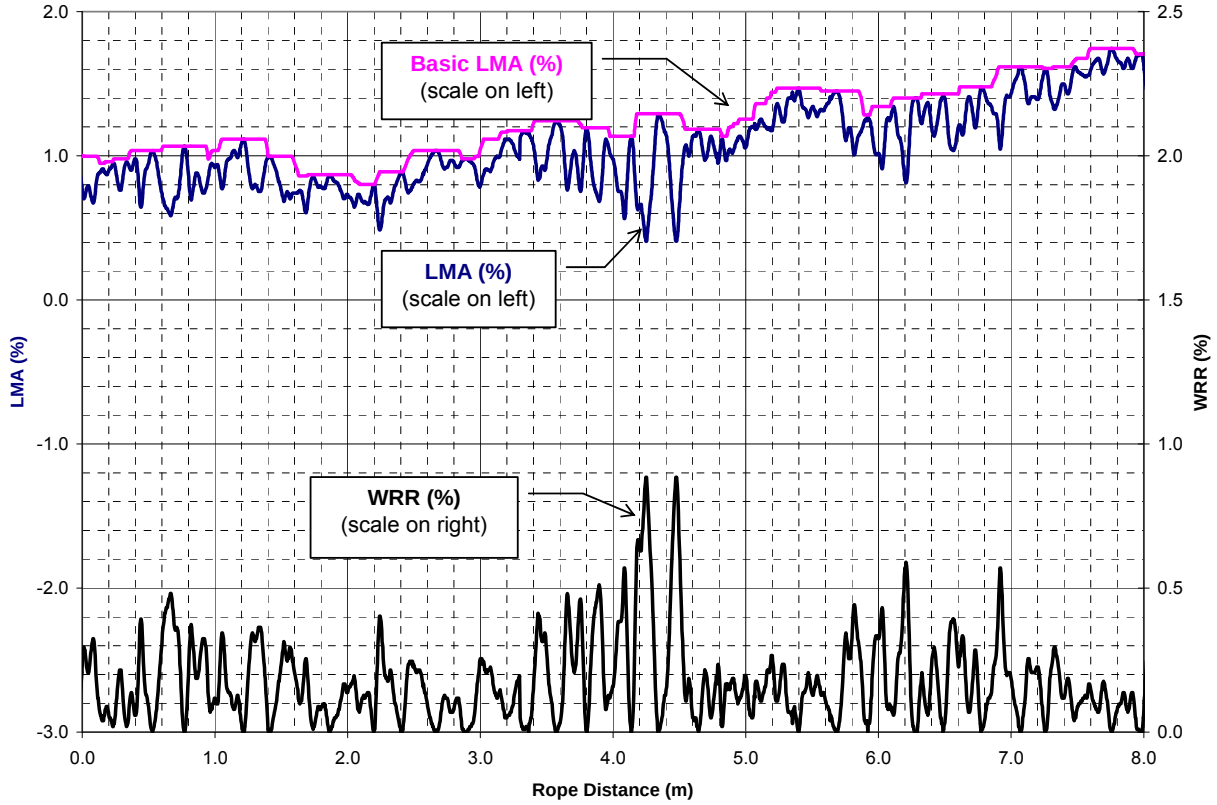

Figure 15: Rope 1, WRR analysis

Figure 16 shows a comparison of the actual WRR values with a visual count of the maximum number of broken wires within a 50 mm sliding window over 0.1m intervals along the length of the rope as published in the Appendix of Reference [**6**].

Note that the test data that were acquired during the nondestructive inspection showed distance measurement errors. These deviations are systematic and cumulative. They can be caused by a slightly oversized or undersized distance counter wheel, slippage of the wheel and many other causes.

The WRR trace in Figure 16 was adjusted to compensate for these distance counter errors. Note that Figure 16 has two distance axes on the top and the bottom of the chart. The axis on the bottom shows the actual distance along the rope as determined during the visual inspection. The top axis shows the rope distance that was measured during the nondestructive inspection. The measured distance axis was adjusted as shown, simply by aligning the peaks of the WRR trace with the peaks of the broken wire trace.

After this alignment, Figure 16 shows a close correlation between test results and the actual number of internal broken wires.

.

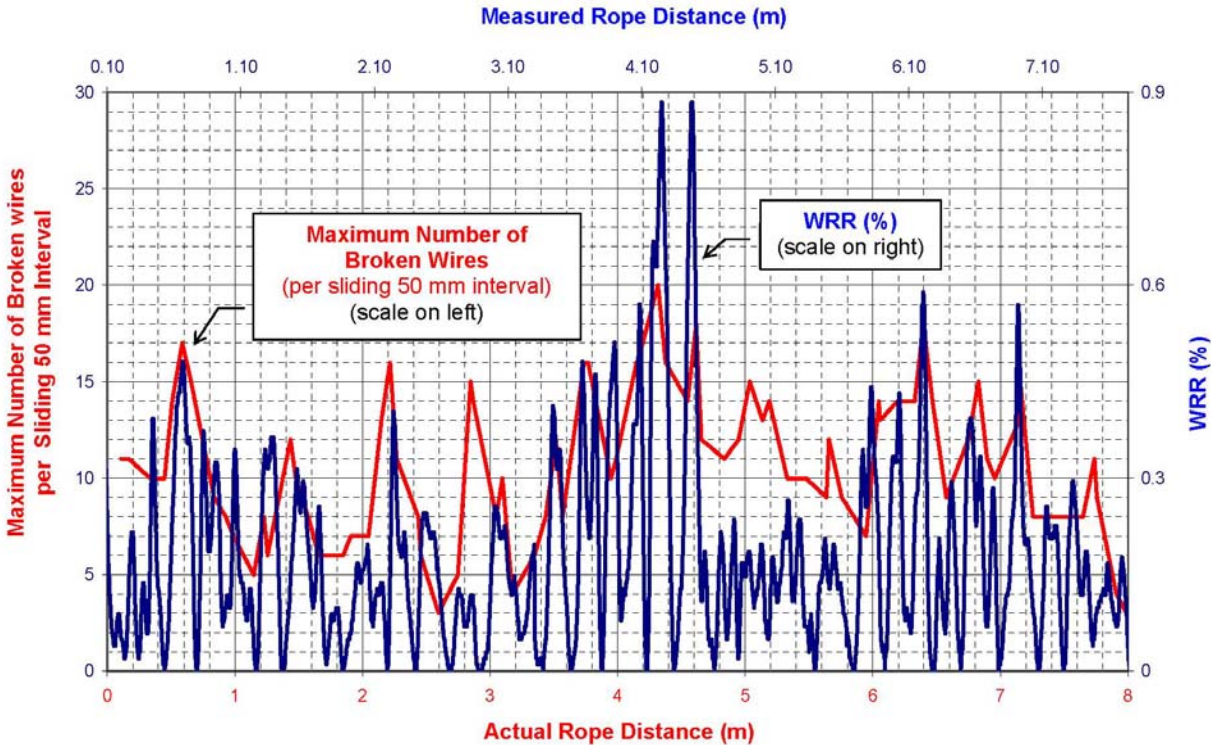

Figure 16: Rope 1, comparison of WRR Analysis results vs. actual broken wire count (distance adjusted)

There are, however, some discrepancies between the test results and the actual broken wire count. These differences can be caused by the fact that the indication of broken wires is influenced by parameters like broken wire gap width, broken wire cross-sectional area, and, most importantly, by the fact that broken wires with zero or tight gap widths are not detectable by nondestructive magnetic inspections because they do not produce a sufficient magnetic leakage flux.

Considering these uncertainties associated with evaluating the combined effects of broken wires, interstrand nicking and internal wear, the accuracy of these nondestructive test results must be considered excellent.

It is even to be expected that the WRR test results, rather than the number of counted broken wires, are a better reflection of the actual rope condition. This is true because, beyond the number of broken wires, the WRR Analysis also reveals and measures other rope deterioration such as interstrand nicking, fretting, wear, etc. In addition, it could be argued that wider gap widths of broken wires indicate more serious rope deteriorations.

Note that, although this rope is in a seriously degraded condition, its LMA trace indicates little change of rope cross-sectional area [**4**]. Only the WRR Analysis exposes the dangerous state of this rope

Furthermore, the dictionary defines *resolution* as "*the level of detail that can be distinguished in an image (or a recording)*." In nondestructive testing, the terms *resolution* and *inspection accuracy* are often used synonymously.

In the discipline of nondestructive magnetic wire rope inspection, *quantitative resolution* or *averaging length* (sometimes also called *scanning length*) is defined as the minimum length of a uniform anomaly for which the sensor provides an accurate measurement of LMA [**2**].

The rope inspection equipment used for acquiring the experimental data of this report – after signal enhancement – offers a *quantitative resolution* of 50 mm.

On the other hand, Appendix 1 of Reference [**6**] lists the number of broken wires in 10 mm intervals along the length of Rope 1. To make the broken wire count commensurate with the quantitative resolution of the test equipment, this data was used to determine the number of broken wires over a 50 mm sliding interval along the length of the rope.

Figure 17 shows the correlation between the broken wire count and the WRR_P values.

Here WRR_P denotes the peak values of WRR. This is an alternative representation of WRR that is used to keep Chart 17 uncluttered.

Similar to Chart 16, distances of the WRR and the broken wire traces were adjusted in Figure 17 by aligning peaks of both traces. This was done by slightly changing the scaling of the *measured distance* axis.

The figure shows a correspondence between the WRR_P trace and the actual broken wire count.

Furthermore, similar to Figures 15 and 16, WRR_P indicates that the rope deterioration in the area around a rope distance of 3.5 to 4.5 m is more serious than indicated by the broken wire count.

This example and the two following tests suggest that ropes should be retired when their WRR exceeds a value of 1% - 2%.

Finally and most importantly, the close correlation between the WRR Analysis and the actual condition of the rope test sample verifies convincingly the value and reliability of the WRR Analysis method.

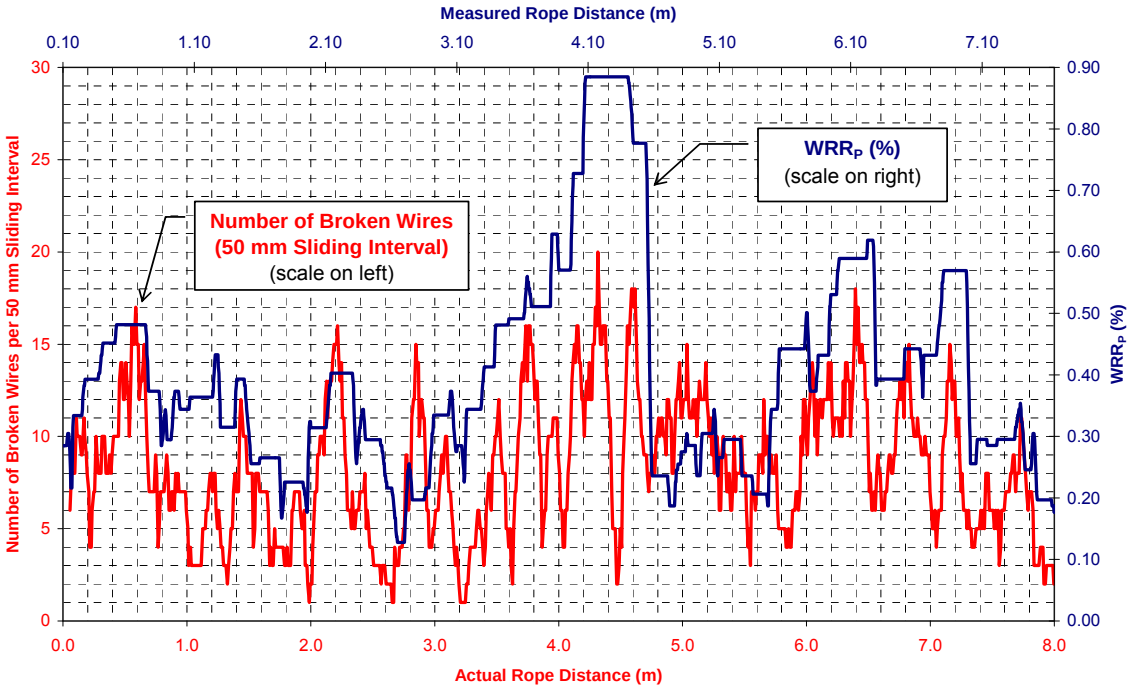

Figure 17: Rope 1, comparison of broken wire count vs. WRR_p (distance adjusted)

4.2 Test 2

This test concerns a 36 mm diameter, 21 strand – 21 (9 x 6 x 6) construction, multilayer, low rotation rope (Figure 18) [6]. The rope will be referred to as Rope 2 in the following.

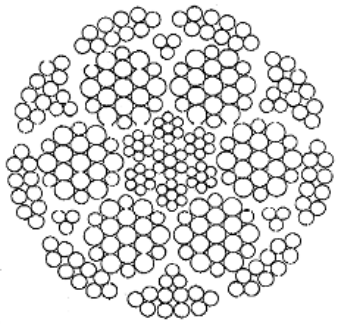

36 mmΦ / 21 Strand / Non-Spin / IWRC
Multistrand Rope

Figure 18: Multistrand rope construction

Rope 2 was in very good condition except for an approximately 3 m length exhibiting heavy corrosion.

Figure 19 shows an inspection chart recording of the corroded section. The chart is used to show the inspection results before and after *signal enhancement*. As mentioned above, the so-called *echo effect* convolutes the LMA signal. However, the signal can be de-convoluted by the above mentioned *echo cancellation* or *signal enhancement* algorithm.

To facilitate a side-by-side comparison of the LMA signal before and after enhancement, the two traces are overlaid. Note that, compared to the acquired signal, the enhanced signal has noticeably better resolution. In other words, the enhanced signal reveals more details of the rope condition.

This is important for the following WRR Analysis that relies on a high-resolution signal in order to make the rope inspection accurate and reliable. Furthermore, the maximum LMA values indicated by the enhanced signal are slightly higher and more accurate than those of the unprocessed signal.

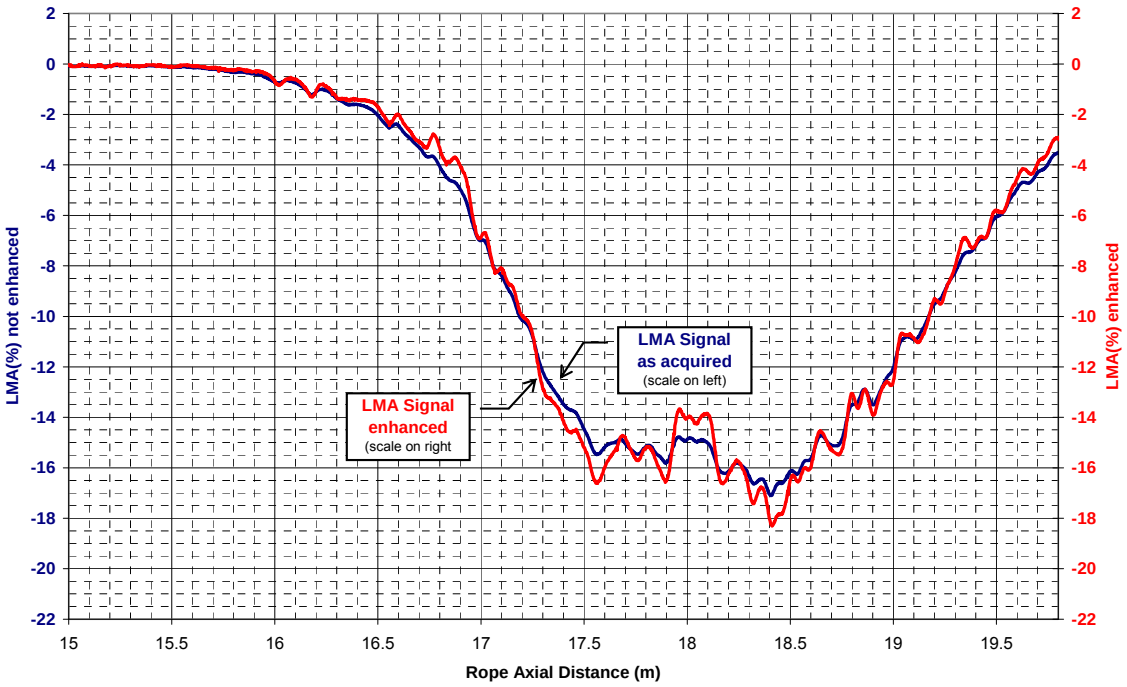

Figure 19: Rope 2, LMA signal before and after echo cancellation

Figure 20 shows the WRR Analysis of Rope 2. Both traces of the chart show severe corrosion. Here, the LMA signal indicates an 18% cross-section loss, while the WRR trace indicates a wire rope roughness of over 3%. By all accepted retirement criteria, this degree of deterioration warrants discard of Rope 2.

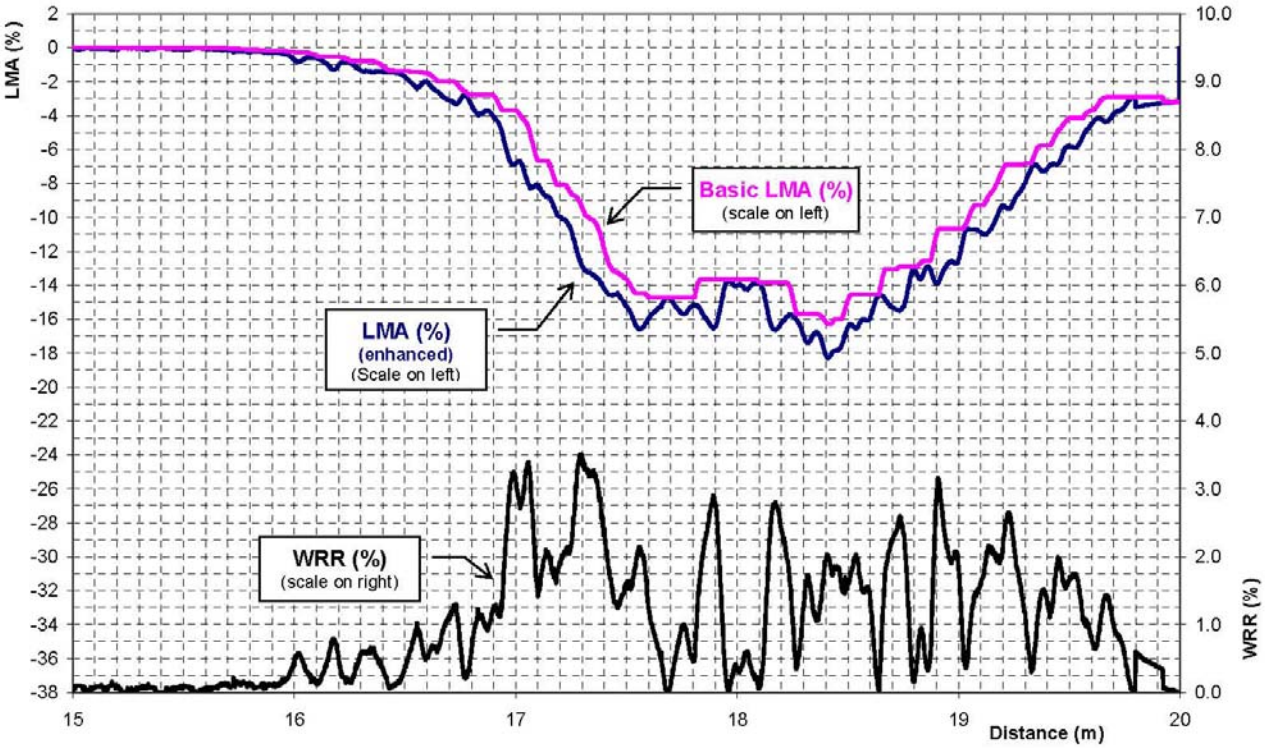

Figure 20: WRR Analysis of Rope 2

4.3 Test 3 [7]

For this test, a 32 mm locked coil rope, left hand lay rope was used. Figure 21 shows its construction.

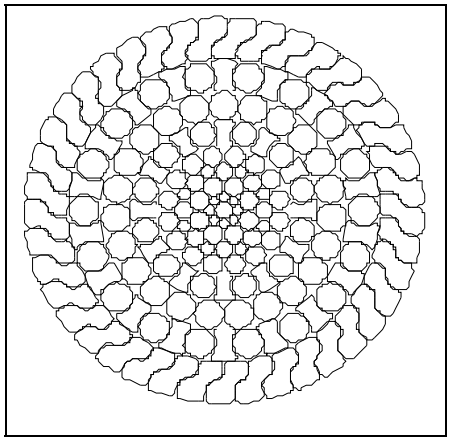

Figure 21: Locked Coil rope construction

This locked coil rope was mounted on a mobile winch for approximately 10 years after 3 months earlier use on a friction winder installation. Its cross-sectional diagram is shown in Figure 21. The rope showed clear evidence of external corrosion, variable along the test length. Using retirement criteria that are appropriate for visual inspections, this rope would have been rejected for further use. Due to its service history the rope was not believed to contain any internal broken wires.

Examination after dismantling. After dismantling, the rope showed severe corrosion on the outer layer and also significant corrosion on the second layer. The third layer showed less corrosion, and from the fourth layer onward the rope appeared undamaged, because lubricants were still present. No broken wires were found (see Figures 22 and 23).

Figure 22: Corrosion in the first and second layer of the rope

Figure 23: Corrosion in the second and third layer of the rope

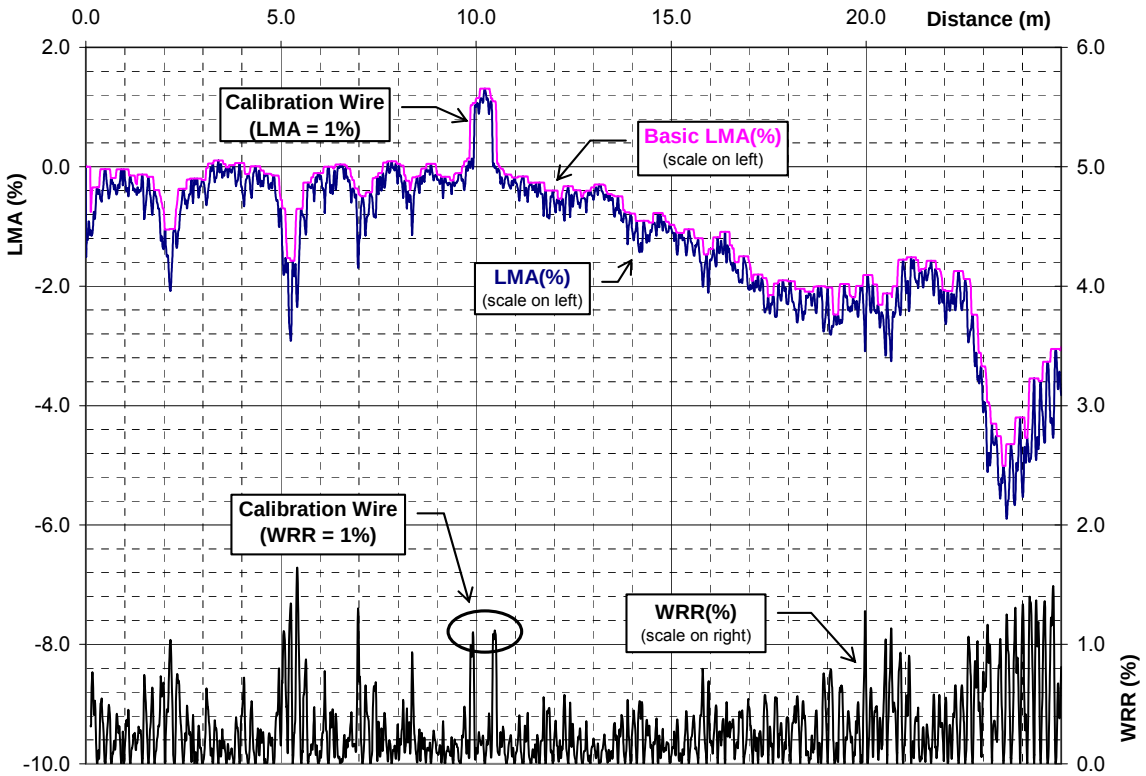

Figure 24: WRR Analysis of Rope 3

Findings of nondestructive magnetic inspection. Figure 24 shows an inspection chart, including WRR Analysis, of this rope. The maximum measured LMA is almost 6% compared to the best section on the rope covered by the chart.

The deterioration pattern indicated to the left of the chart is typical for ropes that wind on a drum with the worst deterioration occurring at the crossover points as the rope slips from layer to layer while winding on a multilayer drum.

Note that the most convenient calibration method for EM inspections is to attach a calibration wire with known cross-sectional area to the rope. In the present case, a wire bundle that represents about a 1% increase in rope cross-section was taped to the rope and used for calibration. This is indicated in the chart.

The WRR signal is extracted from the LMA signal, and the WRR Analysis method is designed in such a way that the LMA as well as the WRR signal are calibrated simultaneously. This feature is illustrated by Figure 24. It shows that, while the calibration wire bundle represents a 1% increase of cross-sectional area, both ends of the wire bundle show a corresponding 1% WRR as indicated in the chart.

Rope 3 shows a maximum LMA of about 6%. This is less than the typical 10% LMA limit that is frequently used as a retirement condition. On the other hand, retirement based on a visual inspection after rope destranding was well justified.

The chart recording in Figure 24 shows a maximum WRR of about 1.6% at a rope distance of 5.4 m. This result, together with the previous tests, suggests that a WRR value of 1% - 2% could be used as a retirement criterion for a rope that shows signs of corrosion pitting and/or internal broken wire clusters.

5 Summary and conclusion

Methods for nondestructively characterizing wire rope degradation that is caused by internal corrosion pitting and clusters of broken wires have not been available in the past.

To improve this situation, the present paper introduces a new concept called *Wire Rope Roughness (WRR)* defined as the surface roughness of the aggregate wires of a rope, including broken wires and corrosion pitting. For individual wires, roughness is defined as the high spatial frequency, short spatial wavelength component of wire surface variations.

A new method for extracting WRR from the LMA signal is presented. The stages of the WRR analysis process are:

- Rope inspection and acquisition of a *high-resolution* LMA signal.
- Using the distance counter signal to produce a distance-based LMA signal.
- Removing measurement artifacts from the LMA signal by using the so-called *echo cancellation (signal enhancement)* algorithm to produce a *high-fidelity* LMA signal.
- Extracting a *high-fidelity* WRR signal from the *high-fidelity* LMA signal by a nonlinear, high-pass filter-like algorithm.

5 References

[**1**] Weischedel, H.R., Chaplin, C.R. “The Inspection of Offshore Wire Ropes: The State of the Art.” OTC 6969, Presented at 24th Annual Offshore Technology Conference, Houston, TX, May 4-7, 1992.

[**2**] Weischedel, H.R. “Magnetic Flux Leakage Inspection of Wire Rope.” Nondestructive Testing Handbook, Third Edition, Volume 5, Electromagnetic Testing, American Society for Nondestructive Testing (2004), pp. 437-450.

[**3**] Ridge, I.M.L., “Tension-Torsion Fatigue Behavior of Wire Ropes for Offshore Applications.” International Journal of Rope Science and Technology, No. 100, December 2010, pp. 17– 41.

[**4**] Dohm, M. “Closure by the Author to discussion of: An evaluation of international and local magnetic rope testing instrument defect detection capabilities and resolution, particularly in respect to low rotation, multilayer rope constructions.” O.I.P.E.E.C. Bulletin 79, June 2000, pp. 55 - 57.

[**5**] Weischedel, H.R., “Electromagnetic Wire Rope Inspection: Signal Generation, Filtering, and Computer-Aided Rope Evaluation.” Presented at The Nondestructive Testing of Rope. Krakow, Poland: (O.I.P.E.E.C.) International Organization for the Study of the Endurance of Wire Rope. (September 1999). Also: O.I.P.E.E.C. Bulletin 79, June 2000, pp. 91 – 104.

[**6**] Dohm, M. "An evaluation of international and local magnetic rope testing instrument defect detection capabilities and resolution, particularly in respect to low rotation, multilayer rope constructions". Project Number GAP 503 and GAP 353. Johannesburg, South Africa: Safety in Mines Research Advisory Committee (1999), pp. 36 - 59. Also: O.I.P.E.E.C. Bulletin 79, June 2000, pp. 55 - 57

[**7**] Smith, D.T., McCann, P. “Evaluation of Instruments for the Non-Destructive Testing of Wire Ropes.” Report No. Fe/02/07. Health and Safety Laboratory, Sheffield, UK, 2002, pp. 35-39.